Design and Evaluation on Electric Differentials for Overactuated Electric Ground Vehicles With Four Independent In-Wheel Motors

Yan Chen and Junmin Wang, *Member, IEEE*

***Abstract*—This paper discusses the design and evaluation of electric differentials (ED) for overactuated electric ground vehicles (EGVs) with four independent in-wheel motors. Three patterns of ED, namely, 1) front ED, 2) rear ED, and 3) all-wheel ED, are designed and discussed based on vehicle performances during normal cornering and circling maneuvers. Through both simulation and experimental results, the three different ED can achieve almost the same vehicle performances in terms of the EGV sideslip angle, yaw rate, and trajectory. Moreover, when an ED is applied to only one pair of wheels, i.e., either the front or rear pair, the other pair of wheels can be utilized to estimate (the passive tires are adopted as sensors under normal driving conditions) the EGV longitudinal speed and yaw rate and consequently generate the reference wheel speeds for the ED wheels. Thus, sensors for measuring the vehicle speed and yaw rate to generate the reference wheel speeds in the design of ED, such as the all-wheel ED design for the EGV, may become unnecessary. Both simulation and experimental results validate the designs of the three ED.**

***Index Terms*—Electric differentials (ED), electric ground vehicle (EGV), in-wheel motor, overactuated.**

I. Introduction

INCREASINGLY stringent standards on vehicle emissions and fuel economy have made hybrid electric vehicles (HEVs) and/or plug-in HEVs (PHEVs) increasingly more attractive to both the industrial and academic communities [1]–[4]. Not only various HEVs and/or PHEVs, such as the Toyota Prius and the Ford Escape, have already entered mass production, but the tendency toward pure electric ground vehicles (EGVs) has also been significantly accelerated by various electrified systems and technologies instead of the conventional mechanical/hydraulic counterparts. For example, regenerative braking can transfer the vehicle kinetic energy into battery electrical energy during the deceleration processes and consequently reduce energy loss from frictional heat in traditional mechanical/hydraulic brakes [5], [6]. In-wheel electrical motor control [7]–[9] is also a novel technology that provides faster and more accurate torque actuation.

Electric differential (ED) is another electrified technology that eliminates the traditional mechanical differentials (MDs) [10]–[12]. An ED system can reduce the weight and friction loss in the drive train by removing MD components and consequently improve the overall reliability and efficiency during the power transmission. The working principle of an ED system is similar to that of a traditional MD. When an EGV is cornering or making a turn, the outer wheels will travel longer paths than the inner ones, implying that the rotational speed of the outer wheels will be faster than that of the inner wheels. The resulting speed differences between the inner and outer wheels are automatically tuned by an ED system. Note that an ED system in an EGV with independently actuated in-wheel motors is essentially a wheel speed tracking control module, which is different from the direct torque control of in-wheel motors.

Various ED designs with different emphases were proposed in the literature [13]–[17]. Yang and Xing [13] proposed an ED system for dual motors in rear wheels consisting of one outer loop for yaw rate control and one inner loop for wheel speed tracking. Haddoun *et al.* [14] discussed an ED design for two independent rear wheels based on a neural network control of induction motors. Pinal *et al.* [15] considered the stability issue by taking into account sudden changes/perturbations on each wheel in the design of an ED for two rear motors with fixed gears. Chen *et al.* [16] designed an ED system for two rear in-wheel motors of a three-wheeled welfare vehicle and the reference wheel speeds were obtained from the Ackerman geometry. Tabbache *et al.* [17] described an adaptive ED structure for two induction motors connected to two front wheels. From the aforementioned descriptions, most literature discussed the ED designs for EGV with only two in-wheel driving motors, which were separated from the steering wheels. Moreover, the ED designs often assumed or required accurate measurements of vehicle speed and yaw rate to generate the reference wheel speeds for synchronization.

In this paper, ED designs for an overactuated EGV with four independent in-wheel motors are discussed. Different from the ED designs in the existing literature, an EGV actuated by four in-wheel motors actually needs two ED for front two wheels and rear two wheels, respectively. If only two wheels are actuated, the ED effects for two front wheels and for two rear wheels are described, considering that the front wheels are steering wheels. The main contributions of this paper are listed

Manuscript received August 5, 2011; revised November 30, 2011 and January 29, 2012; accepted February 7, 2012. Date of publication February 14, 2012; date of current version May 9, 2012. This work was supported in part by the Office of Naval Research Young Investigator Program Award under Grant N00014-09-1-1018, by the Honda–Ohio State University (OSU) Partnership Program, and by the OSU Transportation Research Endowment Program. The review of this paper was coordinated by Prof. L. Guvenc.

The authors are with the Department of Mechanical and Aerospace Engineering, The Ohio State University, Columbus, OH 43210 USA (e-mail: chen.1843@osu.edu; wang.1381@osu.edu).

Color versions of one or more of the figures in this paper are available online at http://ieeexplore.ieee.org.

Digital Object Identifier 10.1109/TVT.2012.2187940

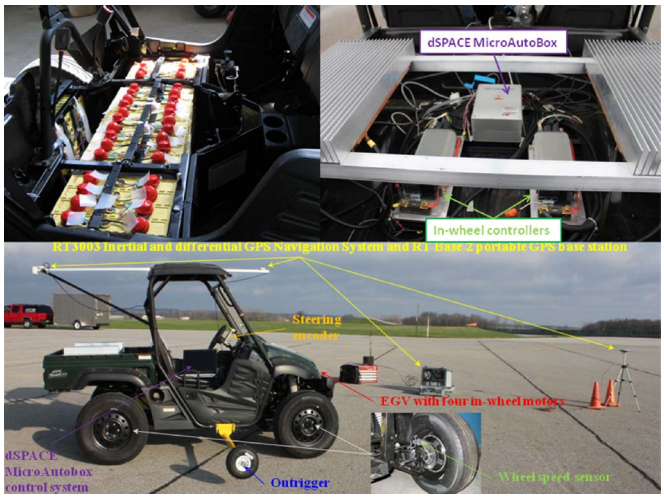

Fig. 1. Configuration of the EGV with four independent in-wheel motors.

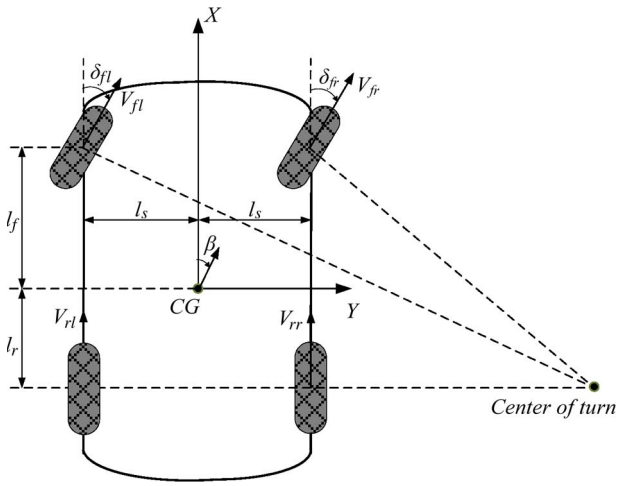

Fig. 2. Kinematic model of an overactuated EGV in a turn maneuver.

as follows: 1) three different ED designs of an overactuated EGV, namely, a) front ED, b) rear ED, and c) all-wheel ED, are proposed and compared based on vehicle performances during normal cornering and circling maneuvers; and 2) the front and rear ED for similar vehicle performance show the advantages of utilizing the estimation of vehicle longitudinal velocity and yaw rate from the passive wheels, without relying on the measured signals from expensive global positioning system (GPS) and/or other additional measurement systems for the all-wheel ED.

The remainder of this paper is organized as follows. In Section II, the kinematic and dynamic models for ED designs are described. Three different EDs are proposed for an EGV with four independently actuated in-wheel motors in Section III. Simulation results and comparisons of three different EDs are discussed in Section IV. In Section V, experimental results validate the designs of three different EDs and confirm the conclusion from the simulation results. Concluding remarks are presented in Section VI.

II. Kinematic and Dynamic Models for Electric Differential Designs

In this section, the configuration of an overactuated EGV, which is adopted as the experimental platform for the ED designs, will be first introduced. Then, the related kinematic and dynamic models for the ED designs will be described. The importance and necessity of an ED module for an EGV with independently actuated in-wheel motors will be demonstrated with a preliminary comparison between two high-speed cornering maneuvers: with and without an ED.

A. EGV Configuration

As shown in Fig. 1, the developed EGV consists of the following five main parts: 1) vehicle body and suspension—directly modified from a commercial utility terrain vehicle; 2) power source—a 72-V LiFeYPO4 battery pack with a battery management system; 3) actuators—four in-wheel motors with independent controllers; 4) sensing systems—an RT3003 high-end navigation system with a dual-antenna differential GPS and four independent wheel speed sensors; and 5) vehicle controller—a dSPACE MicroAutoBox as the real-time vehicle controller. Other mechanical and electrical modifications/designs are discussed in detail in [18].

B. Kinematic and Dynamic Models

As shown in Fig. 2, the linear velocities of the four wheels are represented by V_{fl}, V_{fr}, V_{rl}, and V_{rr}, respectively. The steering angles of front wheels are shown as δ_{fl} and δ_{fr}. The distances from the front wheel and the rear wheel centers to the EGV center of gravity are shown as l_f and l_r. Half of the vehicle track is represented by l_s.

Based on the kinematic model showing in Fig. 2, the linear velocities of the four wheels are described as follows [19], [20]:

$$\begin{aligned} V_{fl} &= (V_x + rl_s)\cos\,\delta_{fl} + (V_y + rl_f)\sin\,\delta_{fl} \\ V_{fr} &= (V_x - rl_s)\cos\,\delta_{fr} + (V_y + rl_f)\sin\,\delta_{fr} \\ V_{rl} &= V_x + rl_s \\ V_{rr} &= V_x - rl_s \end{aligned} \tag{1}$$

where V_x, V_y, and r are vehicle longitudinal speed, lateral speed, and yaw rate, respectively. Assume that all the tires have the same effective radius R_{eff}. The reference rotational speed of each wheel during a turn maneuver is described in the following:

$$\omega_{fl} = \frac{V_{fl}}{R_{\text{eff}}},\ \omega_{fr} = \frac{V_{fr}}{R_{\text{eff}}},\ \omega_{rl} = \frac{V_{rl}}{R_{\text{eff}}},\ \omega_{rr} = \frac{V_{rr}}{R_{\text{eff}}}. \tag{2}$$

The vehicle longitudinal dynamics is represented as

$$m\dot{V}_x = 2F_{xf} + 2F_{xr} - F_a \tag{3}$$

where m is the vehicle total mass, V_x is the vehicle longitudinal velocity, and F_{xf} and F_{xr} are the friction forces acting on a front and a rear tire, respectively. F_{xf} and F_{xr} are written separately in (3) because the actuation of the front wheels and rear wheels will be commanded independently in the later ED designs. The rolling resistances are negligible here compared

with the large ground friction forces. The aerodynamic drag force F_a is modeled as [19]

$$F_a = C_{av} V_x^2 \tag{4}$$

where C_{av} is the aerodynamic coefficient.

Each of the in-wheel motors is a brushless DC motor, whose dynamics can be approximately treated as a common DC motor, i.e.,

$$\begin{aligned} J\dot{\omega}_i &= T_{ei} - T_{fi} - F_{xi} R_{\text{eff}} \\ T_{ei} &= K_i I_i \\ T_{fi} &= p\omega_i. \end{aligned} \tag{5}$$

The subscript $i = f$ or r in (5) stands for one front or rear motor of the vehicle, and J is the combined rotational inertia of the wheel and in-wheel motor. T_{ei} is the electromagnetic torque generated by the motor current I_i, and T_{fi} is the motor viscous frictional torque with the viscous coefficient being p. K_i and ω_i are the back electromotive force constant and rotational speed of the motor, respectively. Note that the motor frictional torques T_{fi} in (5) can be experimentally characterized and overcome by the motor electromagnetic torque. The relationship between the motor control signal and the motor output torque can thus be calibrated by experimental data [18]. For other characteristics of the in-wheel motor, see [18].

C. Importance and Necessity of an ED

To show the importance and necessity of the ED design for an overactuated EGV, the following simulation results display the difference between two high-speed cornering maneuvers with and without an ED.

As shown in Fig. 3, an overactuated EGV is actuated by two rear motors to cruise at a constant speed of 50 km/h. The input hand-steering angle linearly increases to 70° within 5 s. Since the gear ratio from the hand-steering wheel to the front driving wheels is about 14, the maximum steering angles for both front wheels (assumed to be the same) can reach 5°. When the EGV follows a cornering and then circling maneuver, the trajectory with an ED shows a smaller circle than that without an ED. Although the speed tracking effect of the EGV with an ED is a little bit worse than the case without an ED, the yaw stability, which is shown by the sideslip angles, is considerably enhanced in the case of ED. The reason is shown by the torque distributions. The cruise with ED shows different torque distributions between the rear two driving motors. While the cruise without ED exerts an equal torque distribution to the two driving motors, which makes the yaw stability worse during circling. Moreover, the yaw rate responses for both cases are almost the same, which shows that the introduced torque differences by the rear ED do not make the yaw rate response worse on behalf of a smaller sideslip angle. Although the EGV is still stable as shown in Fig. 3, the cruising without ED become unstable when higher speed and/or larger steering angle is required, which is shown in Fig. 4.

As shown in Fig. 4, in both large steering angle and high speed cornering cases, the vehicle becomes oversteering and

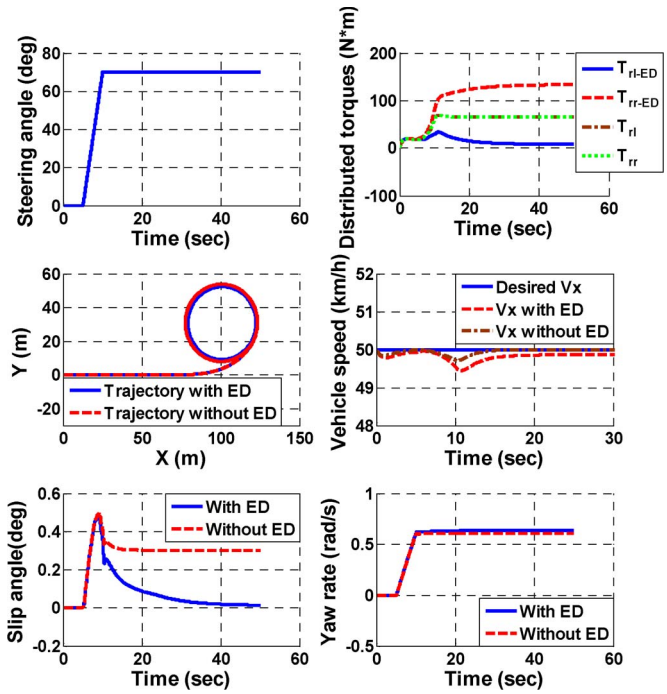

Fig. 3. Example on cornering and circling trajectories of an overactuated EGV with and without rear ED.

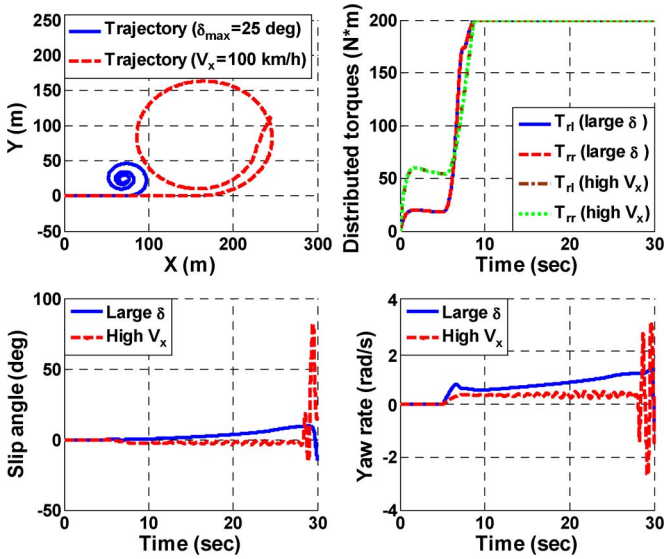

Fig. 4. Unstable simulation results due to a large steering angle or a high cornering speed without ED.

quickly unstable observed from the sideslip angle and yaw rate responses. Meanwhile, the rear driving torque levels reach the maximum values due to the actuation limitations of the in-wheel motors.

III. Three Electric Differentials for an Overactuated Electric Ground Vehicle

For an overactuated EGV with four independent in-wheel motors, the ED design can be applied to front two wheels, rear two wheels, or all four wheels since the EGV can be actuated in front-wheel drive, rear-wheel drive, or all-wheel drive modes.

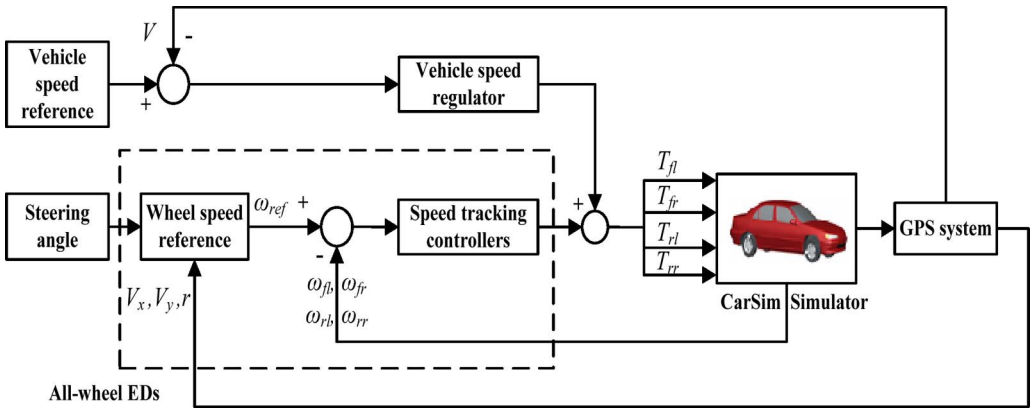

Fig. 5. Configuration of the all-wheel ED design.

In this section, these three different ED structures are designed. For different ED configurations, the required measurements and, consequently, the control structures are distinct.

A. All-Wheel ED

When the EGV is driven by all four wheels in a cornering maneuver, the inner two and outer two wheels will have different rotational speeds. Thus, one ED for the front two wheels and the other for the rear two wheels need to be designed.

As shown in Fig. 5, the all-wheel ED configuration consists of three main parts. The first one is a high-level speed regulation controller for maintaining a constant vehicle speed during the cornering. Note that the vehicle speed regulation controller is applied to assist and compare the three ED designs, and it realizes the same vehicle speed for different designs. The second part consists of two EDs for the front and rear wheels, respectively. The EDs are realized through four wheel speed tracking controllers. The reference wheel speeds are given in (1) and (2). The third part is the GPS sensing system, which gives the real-time vehicle longitudinal speed, lateral speed, and yaw rate for the high-level vehicle speed regulation and generating the wheel speed references. The GPS signals for CarSim integrated simulations are directly obtained from the CarSim outputs, which represent accurate signals similar to that measured by a GPS. Note that the real-time signals are fed back to generate the reference wheel speed signals under normal driving conditions. Since the ED designs are intended to enhance the drivability of the EGV instead of using traditional MDs, the EDs are different from the yaw motion stabilization systems, and the stable and safe maneuvers are assumed to be generated by a driver or high-level vehicle stability control systems.

Since all the wheels are actuated for driving, the additional GPS/inertia measurement systems are required to produce accurate vehicle speed and yaw rate signals for the ED design. The usage of such measurement systems actually has two main disadvantages. The first one is that the current cost of an accurate GPS/inertia measurement system (e.g., the RT3003 used in the experiments) is high and not acceptable by production applications. The second disadvantage is that the GPS-based measurement system is generally unreliable in urban and forested driving environments where tall buildings, trees, and hills may prevent communications between GPS receivers and GPS satellites. Thus, it is important to be able to estimate the related vehicle states, such as longitudinal speed and yaw rate, for the ED designs without relying on GPS-based measurements. The following front ED and rear ED designs are proposed for this purpose.

B. Front ED

In the front ED design, the synchronization of rotational speeds for front two wheels is considered since only front wheels are actuated and the rear wheels are passive, which are employed as an estimator to generate the required vehicle states for the front ED design.

Before the front ED configuration is introduced, (1) and (2) are combined and rewritten as follows by ignoring the product of vehicle lateral speed and front wheel steering angle since this term is usually negligible during normal cornering maneuvers:

$$\omega_{fl} = \frac{\cos\,\delta_{fl}}{R_{\text{eff}}} V_x + \frac{(l_f \sin\,\delta_{fl} + l_s \cos\,\delta_{fl})}{R_{\text{eff}}} r$$
$$\omega_{fr} = \frac{\cos\,\delta_{fr}}{R_{\text{eff}}} V_x + \frac{(l_f \sin\,\delta_{fr} - l_s \cos\,\delta_{fr})}{R_{\text{eff}}} r \tag{6}$$
$$\omega_{rl} = \frac{1}{R_{\text{eff}}} V_x + \frac{l_s}{R_{\text{eff}}} r$$
$$\omega_{rr} = \frac{1}{R_{\text{eff}}} V_x - \frac{l_s}{R_{\text{eff}}} r. \tag{7}$$

As shown in (6) and (7), the rotational speeds of four wheels are represented as functions of vehicle longitudinal speed and yaw rate. When front wheels are actuated as the driving wheels, the vehicle longitudinal speed and yaw rate can be represented by the rotational speeds of the passive rear wheels by solving V_x and r from (7), i.e.,

$$\begin{bmatrix} V_x \\ r \end{bmatrix} = \begin{bmatrix} \frac{R_{\text{eff}}}{2} & \frac{R_{\text{eff}}}{2} \\ \frac{R_{\text{eff}}}{2l_s} & -\frac{R_{\text{eff}}}{2l_s} \end{bmatrix} \begin{bmatrix} \omega_{rl} \\ \omega_{rr} \end{bmatrix}. \tag{8}$$

From (8), the passive rear wheels are adopted as an estimator to provide the vehicle longitudinal speed V_x and yaw rate r for generating the reference wheel speeds of front wheels. Although the matrix in (8) is assumed to be constant with known R_{eff} and l_s, the measured rotational speed signals of

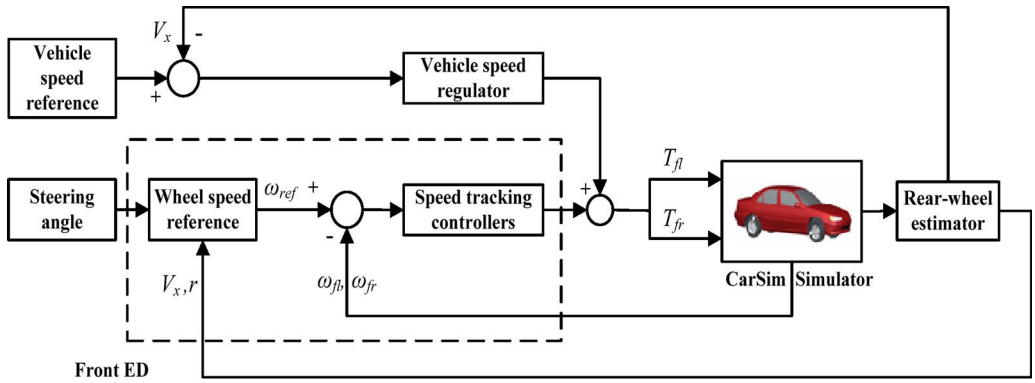

Fig. 6. Configuration of the front ED design.

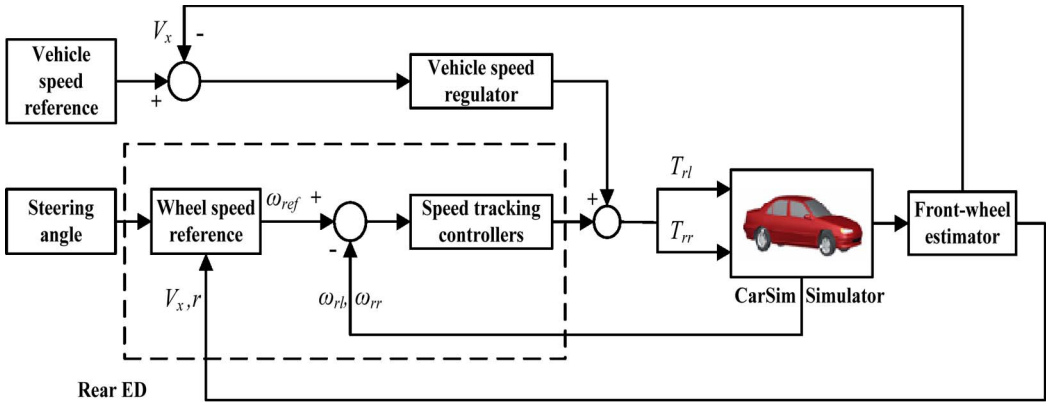

Fig. 7. Configuration of the rear ED design.

rear wheels are usually very noisy in experiments. Thus, a Kalman filter is first applied to obtain relatively smooth wheel speed signals, and then the vehicle velocity and yaw rate are calculated from (8). The structure of the front ED is shown in Fig. 6.

Different from the configuration of all-wheel ED shown in Fig. 5, the rear wheel estimator is adopted instead of a GPS. Moreover, the wheel speed tracking is only for the front two driving wheels. The high-level speed regulation controller for maintaining a constant vehicle speed during the cornering is the same as that for the all-wheel ED case.

C. Rear ED

Similar to the design of the front ED, the synchronization of rotational speed for rear two wheels is only considered in the rear ED design since only the rear wheels are actuated and the front wheels are passive, which are employed as an estimator to generate the required vehicle states for the rear ED design.

Assuming that the steering angles for the front right and left wheels are the same, namely $\delta_{fl} = \delta_{fr} = \delta$, the vehicle longitudinal speed and yaw rate can be represented by the rotational speeds of the passive front wheels by solving V_x and r from (6), i.e.,

$$\begin{bmatrix} V_x \\ r \end{bmatrix} = \begin{bmatrix} \frac{(l_s \cos\delta - l_f \sin\delta) R_{\text{eff}}}{2l_s(\cos\delta)^2} & \frac{(l_s \cos\delta + l_f \sin\delta) R_{\text{eff}}}{2l_s(\cos\delta)^2} \\ \frac{R_{\text{eff}}}{2l_s \cos\delta} & -\frac{R_{\text{eff}}}{2l_s \cos\delta} \end{bmatrix} \begin{bmatrix} \omega_{fl} \\ \omega_{fr} \end{bmatrix}. \tag{9}$$

When the measured wheel speed signals that are filtered through Kalman filters are applied to (9), the vehicle velocity and yaw rate can be obtained. Combined with (7), the reference wheel speeds for rear wheels are obtained. The configuration of the rear ED is shown in Fig. 7.

Different from the configurations of the all-wheel ED and the front ED, shown in Figs. 5 and 6, respectively, the front wheel estimator is adopted instead of the GPS and rear wheel estimator. Moreover, the wheel speed tracking is only for the two rear driving wheels. The high-level speed regulation controller for maintaining a constant vehicle speed during the cornering movement is the same as those for the all-wheel and front ED cases.

IV. Simulation Results and Comparisons

In this section, simulation results based on a high-fidelity CarSim vehicle model for the three proposed ED will be demonstrated. To compare the effects of three ED, the vehicle maneuvers for three ED were kept identical. The EGV will cruise at a constant speed of 30 km/h with the hand-steering wheel angle variations shown in Fig. 8. The ratio from the hand-steering wheel to the front ground wheels was calibrated as 14. Thus, the maximum steering angles for both front wheels are assumed to be the same and can reach 5°, as implied in Fig. 8. The other parameters for the EGV are shown in Table I. For more characteristics and parameters of the simulation plant and the experimental vehicle, see [18].

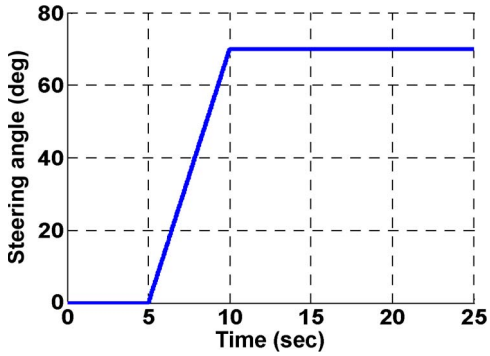

Fig. 8. Variation of the hand-steering wheel angle.

TABLE I
SIMULATION PARAMETERS

Symbol	Parameters	Values
m	vehicle mass	800 kg
C_a	aerodynamic resistance coefficient	0.37
L_f	distance from front wheel to vehicle center of gravity	0.8 m
L_s	half of vehicle width	0.73 m
R_{eff}	tire effective radius	0.33 m
J	combined inertia of a tire and motor	1.5 kg.m^2

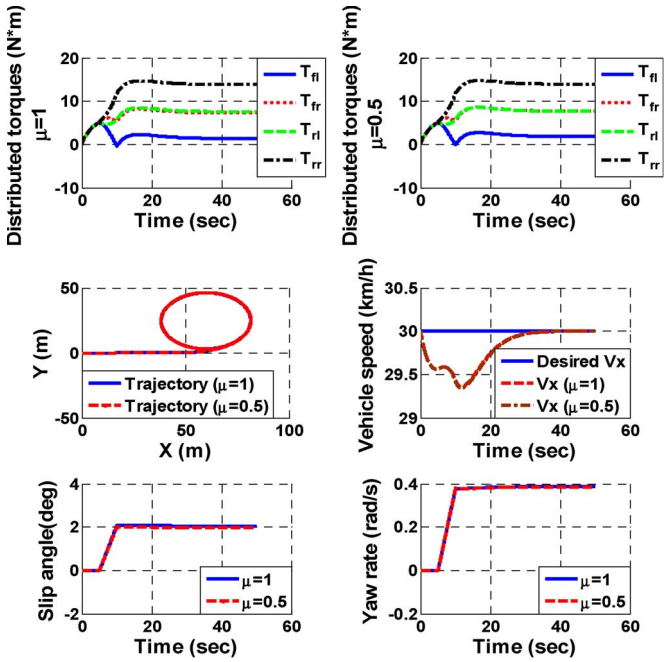

Fig. 9. Simulation results of the all-wheel ED.

A. All-Wheel ED

The simulation results of the all-wheel ED are shown in Fig. 9. Note that since all the four in-wheel motors are applied to drive the EGV, the GPS signals have to be applied to generate the reference wheel speeds in the ED design, following the configuration in Fig. 5. The vehicle speed regulation controller and wheel speed tracking controller are simply proportional–integral (PI) controllers. The parameter tuning process for the PI controllers can be generally described as follows. The PI controller for the vehicle speed regulation was first tuned through the standard Ziegler–Nichols method [21]. Next, the four PI tracking controllers for wheel speeds were designed. Although the control parameter tuning processes also follow the Ziegler–Nichols method, the balance between the regulation control and the tracking control needs to be carefully adjusted. Since the regulation control was mainly adopted to assist the ED designs, namely the wheel speed tracking effect, the control parameter tuning for the vehicle speed regulation error has a higher tolerance than that of the wheel speed tracking error.

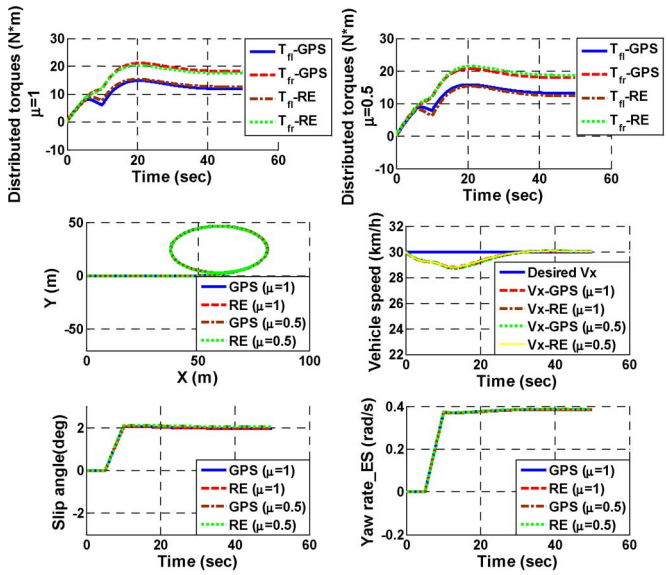

Fig. 10. Simulation results of the front ED.

The cornering and circling motions of the all-wheel ED on both high $(\mu = 1)$ and low $(\mu = 0.5)$ friction road surfaces are shown in Fig. 9. The torque distributions for both high and low friction road surfaces, which are generated from the ED module, are almost the same due to the normal/mild driving maneuvers. If no ED design is adopted, the torque distributions should be equal, similar to that in Fig. 3. The vehicle trajectories for both high and low friction road surfaces are also the same. The constant speed cruises are achieved as well. The steady sideslip angle and the yaw rate during circling for both high and low friction roads are about 2° and 0.4 rad/s, respectively.

B. Front ED

The simulation results of the front ED based on GPS signals and on rear-wheel estimations for both high $(\mu = 1)$ and low $(\mu = 0.5)$ friction road surfaces are compared in Fig. 10. The torque distributions of the front ED based on GPS and rear-wheel estimation for both road surfaces are almost the same. All the four cases have the similar responses in terms of the EGV trajectory, vehicle sideslip angle, and yaw rate. The rear-wheel estimation yaw rates are compared with the GPS measured signals in the last plot in Fig. 10, which verified that the passive rear-wheel estimation can offer the same signals as the accurate GPS measured signals under normal driving conditions.

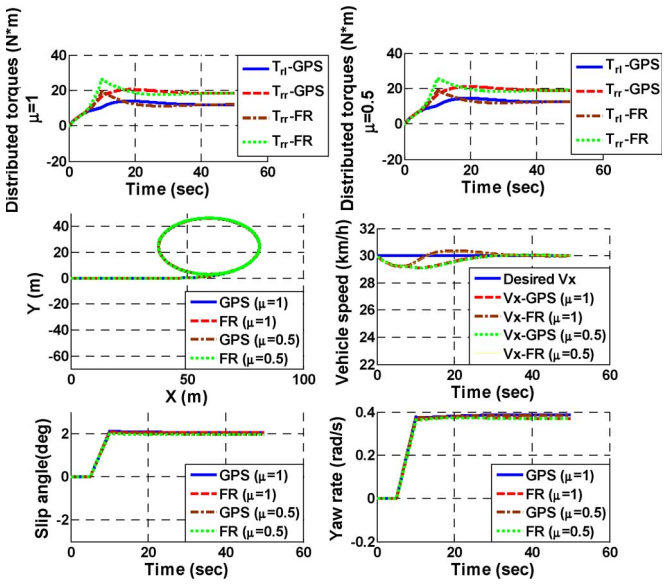

Fig. 11. Simulation results of the rear ED.

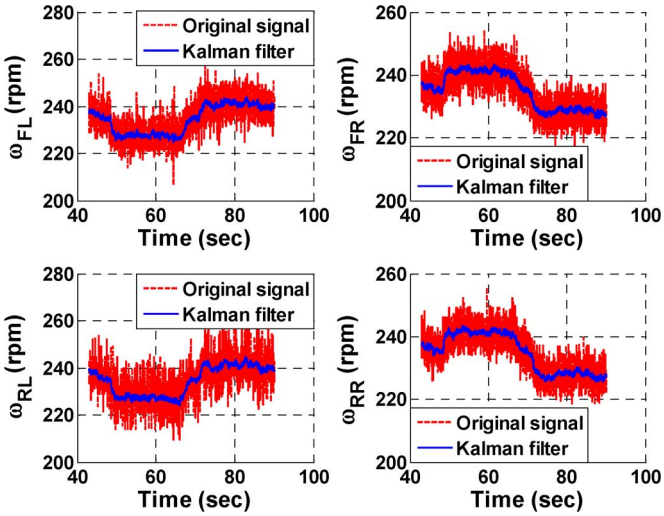

Fig. 12. On-line wheel speed signals before and after Kalman filter implementation.

C. Rear ED

Similarly, the simulation results of the rear ED based on GPS signals and on front-wheel estimations for both high $(\mu = 1)$ and low $(\mu = 0.5)$ friction road surfaces are compared in Fig. 11. As shown in Fig. 11, all the four cases have the similar responses in terms of the EGV trajectory, vehicle sideslip angle, and yaw rate, which verified that the passive front-wheel estimations can offer the same effects as the accurate GPS signals.

V. Experimental Validations and Discussions

In this section, the experimental results are displayed to demonstrate the effects of three ED. The experimental platform, an overactuated EGV with four independent in-wheel motors, is described and shown in Section II. In the experiments, Kalman filters were applied to obtain relatively smooth wheel signals from the measured noisy wheel speed sensor signals for speed feedback in ED.

It is well known that the Kalman filter is a powerful tool to estimate and predict the real signal in the presence of noises [22]. The discrete-time model for the wheel angular velocity and acceleration is expressed as follows:

$$\begin{bmatrix} \omega_{k+1} \\ a_{k+1} \end{bmatrix} = \begin{bmatrix} 1 & T_s \\ 0 & 1 \end{bmatrix} \begin{bmatrix} \omega_k \\ a_k \end{bmatrix} + \tilde{w}_k \tag{10}$$

$$y_k = \omega_k + \tilde{e}_k \tag{11}$$

where ω_{k+1} and a_{k+1} stand for angular velocity and acceleration at time $k+1$. y_k is the output, and $T_s = 0.01$ is the sample time of the dSPACE controller. $\tilde{w}_k$ is the process noise and $\tilde{e}_k$ is the measurement noise. The process noise covariance is calibrated as $S_w = E(\tilde{w}_k \tilde{w}_k^T) = \begin{bmatrix} 0 & 0 \\ 0 & 10^{-4} \end{bmatrix}$ based on the experimental data. Similarly, the measurement noise covariance is calibrated as $S_e = E(\tilde{e}_k \tilde{e}_k^T) = 1$ based on the experimental data. Thus, based on the discrete system model in (10) and (11) and covariance matrices S_w and S_e, the following Kalman filter form is adopted for angular velocity and acceleration estimation:

$$\begin{aligned} K_k &= AP_kC^T(CP_kC^T + S_e)^{-1} \\ \hat{x}_{k+1} &= \begin{bmatrix} \hat{\omega}_{k+1} \\ \hat{a}_{k+1} \end{bmatrix} = A\hat{x}_k + K_k(y_{k+1} - C\hat{x}_k) \\ P_{k+1} &= AP_kA^T + S_w - AP_kC^TS_e^{-1}CP_kA^T \end{aligned} \tag{12}$$

where matrices A and C are the state matrix and output matrix in (10) and (11). The estimation results by using the Kalman filter (12) are shown in Fig. 12.

As shown in Fig. 12, the measured wheel speeds are too noisy to be applied as the feedback signals. However, the signals become suitable after the Kalman filtering. Four wheel speed signals were processed through four Kalman filters and then input into the EDs in the experiments.

A. Rear-Wheel Drive With and Without an ED

The experimental results on cornering and circling maneuvers for the rear wheel drive with and without ED are demonstrated in Fig. 13.

As shown in Fig. 13, the experimental data on rear wheel drive without and with ED (under the GPS feedback) are compared. The transient steering angles are not exactly the same due to the difference on manual steering actions. The constant speed cruising and the yaw rate responses are similar for both cases. However, the sideslip angles and the trajectories of the rear ED case have better experimental results than those of the other case. Moreover, from the torque distributions, it is clear that the rear ED generates an obvious torque difference between rear two wheels, while the rear drive without ED basically produces the equal torque distribution for the two rear wheels.

B. All-Wheel ED

As shown in Fig. 14, the constant speed cruising is regulated well by the vehicle speed regulation controller together with the all-wheel ED module with the accurate GPS feedback. The sideslip angle gradually increases up to 0.5° from 0° along with

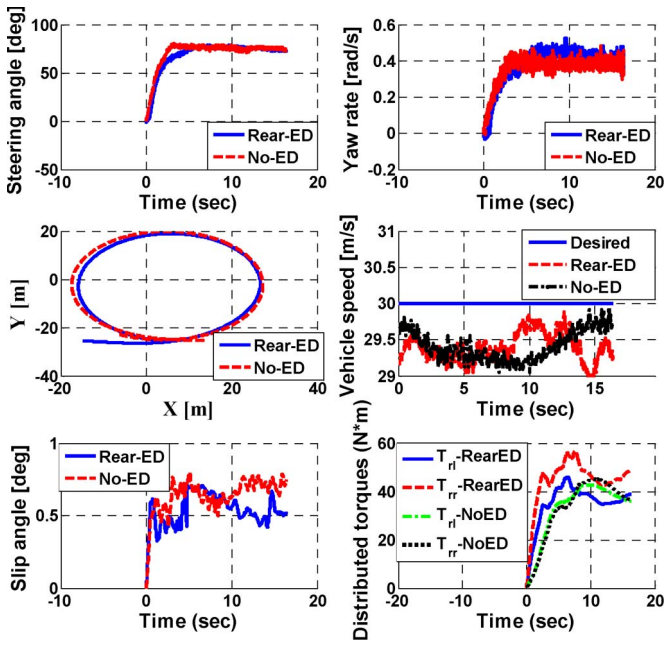

Fig. 13. Experimental results of rear wheel drive with and without rear ED based on GPS feedback signals.

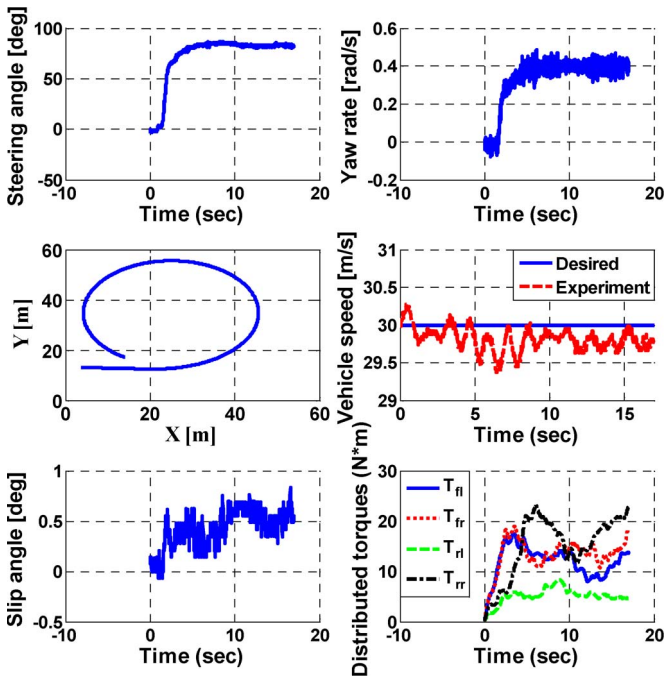

Fig. 14. Experimental results of the all-wheel ED with GPS feedback signals.

the cornering trajectory and stays at about 0.5° during circling. The yaw rate is about 0.4 rad/s. The torque differences due to the all-wheel ED are clearly distributed.

C. Front ED

As shown in Fig. 15, the constant speed cruising is regulated well by the vehicle speed regulation controller together with the front ED utilizing the estimated vehicle states from the passive rear wheels. The sideslip angle gradually increases up to 0.5° from 0°, along with the cornering trajectory, and stays

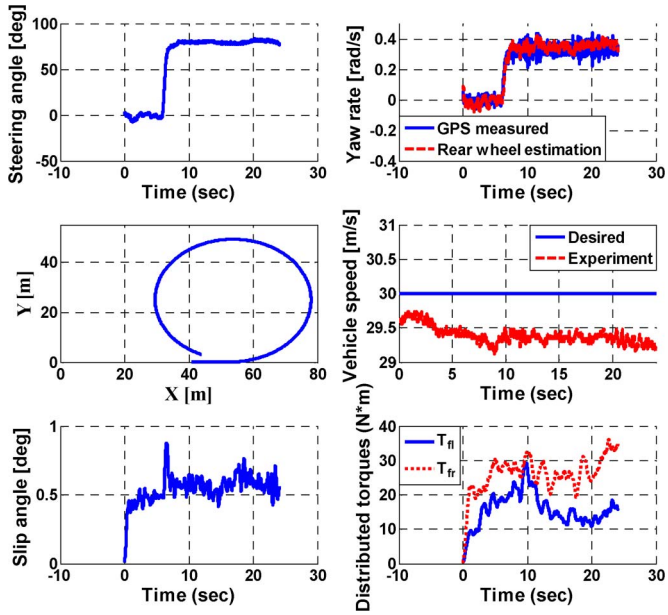

Fig. 15. Experimental results of the front ED based on passive rear-wheel estimation.

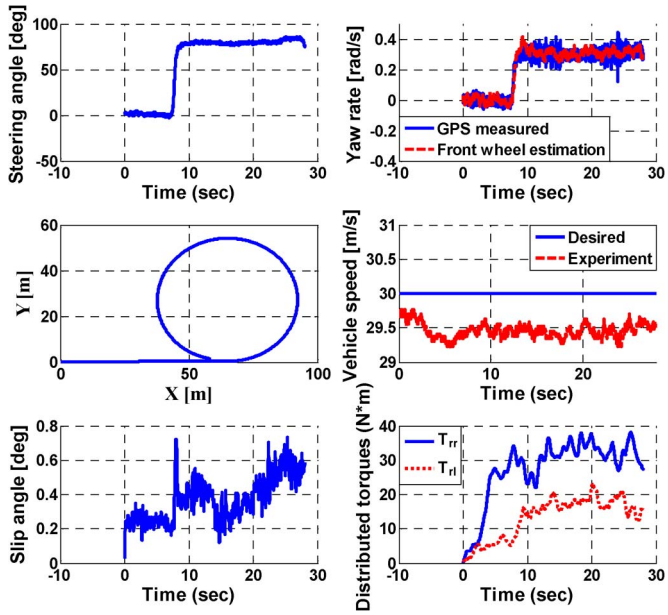

Fig. 16. Experimental results of the rear ED based on passive front-wheel estimation.

at about 0.6° during circling. The estimated yaw rate from the passive rear wheels matches the measured accurate signal of the RT3003 navigation system (an integrated differential GPS and inertial measurement system) well. The torque differences due to the front ED module are clearly distributed.

D. Rear ED

As shown in Fig. 16, the constant speed cruising is regulated well by the vehicle speed regulation controller together with the rear ED utilizing the estimated vehicle states from the passive front wheels. The vehicle sideslip angle gradually increases up to 0.4° from 0°, along with the cornering trajectory, and stays

at about 0.5° during circling. Moreover, the estimated yaw rate from the passive front wheels matches the accurate signal from the RT3003 navigation system well. The torque differences due to the rear ED are clearly distributed.

VI. Conclusion

For an overactuated EGV with four independent in-wheel motors, three different ED, namely, 1) the front ED, 2) the rear ED, and 3) the all-wheel ED, are designed and compared based on vehicle performances on cornering and circling maneuvers. Compared with the all-wheel ED, the front and rear ED can utilize the passive wheels to estimate the vehicle speed and yaw rate for generating the reference wheel rotational speeds from kinematic models and, thus, can offer advantages in applications where GPS-based measurements are not affordable or not available. Both simulation and experimental results validate the design and comparison of three ED under normal driving maneuvers.

Note that the front and rear ED with the passive wheels estimating the vehicle speed and yaw rate are applicable for normal and stable vehicle operations. Under adverse driving conditions where vehicle motions are not stable, the applicability of such ED will be limited.

References

[1] C. C. Chan, "The state of the art of electric, hybrid, and fuel cell vehicles," *Proc. IEEE*, vol. 95, no. 4, pp. 702–718, Apr. 2007.

[2] Y. Chen and J. Wang, "Adaptive vehicle speed control with input injections for longitudinal motion independent road frictional condition estimation," *IEEE Trans. Veh. Technol.*, vol. 60, no. 3, pp. 839–848, Mar. 2011.

[3] R. Wang and J. Wang, "Fault-tolerant control with active fault diagnosis for four-wheel independently-driven electric ground vehicles," *IEEE Trans. Veh. Technol.*, vol. 60, no. 9, pp. 4276–4287, Nov. 2011.

[4] Y. Chen and J. Wang, "Fast and global optimal energy-efficient control allocation with applications to over-actuated electric ground vehicles," *IEEE Trans. Control Syst. Technol.*, 2011, DOI: 10.1109/TCST.2011.2161989, to be published.

[5] M. Ye, Z. Bai, and B. Cao, "Robust control for regenerative braking of battery electric vehicle," *IET Control Theory Appl.*, vol. 2, no. 12, pp. 1105–1114, Dec. 2008.

[6] Y. M. Gao, L. P. Chen, and M. Ehsani, "Investigation of the effectiveness of regenerative braking for EV and HEV," presented at the Soc. Automotive Eng., Costa Mesa, CA, 1999, Tech. Paper 1999-01-2910.

[7] Y. P. Yang, Y. P. Luh, and C. H. Cheung, "Design and control of axial-flux brushless DC wheel motors for electric vehicles—Part I: Multiobjective optimal design and analysis," *IEEE Trans. Magn.*, vol. 40, no. 4, pp. 1873–1882, Jul. 2004.

[8] Y. P. Yang, J. P. Wang, S. W. Wu, and Y. P. Luh, "Design and control of axial-flux brushless DC wheel motors for electric vehicles—Part II: Optimal current waveforms and performance test," *IEEE Trans. Magn.*, vol. 40, no. 4, pp. 1883–1891, Jul. 2004.

[9] G. S. Buja and M. P. Kazmierkowski, "Direct torque control of PWM inverter-fed AC motors—A survey," *IEEE Trans. Ind. Electron.*, vol. 51, no. 4, pp. 744–757, Aug. 2004.

[10] Y. Zhou, S. Li, X. Zhou, and Z. Fang, "The control strategy of electronic differentials for EV with four in-wheel motors," in *Proc. Chin. Control Decis. Conf.*, 2010, pp. 4190–4195.

[11] K. Hartani, M. Bourahla, Y. Miloud, and M. Sekkour, "Direct torque control of an electronic differential for electric vehicle with separate wheel drives," *J. Autom. Syst. Eng.*, vol. 2, no. 2, p. 2, Jun. 2008.

[12] E. Esmailzadeh, G. R. Vossoughi, and A. Goodarzi, "Dynamic modeling and analysis of a four motorized wheels electric vehicle," *Veh. Syst. Dyn.*, vol. 35, no. 3, pp. 163–194, Mar. 2001.

[13] Y. P. Yang and X. Y. Xing, "Design of electric differential system for an electric vehicle with dual wheel motors," in *Proc. 47th IEEE Conf. Decis. Control*, 2008, pp. 4414–4419.

[14] A. Haddoun, M. Benbouzid, D. Diallo, R. Abdessemed, J. Ghouili, and K. Srairi, "Modeling, analysis, and neural network control of an EV electrical differential," *IEEE Trans. Ind. Electron.*, vol. 55, no. 6, pp. 2286–2294, Jun. 2008.

[15] F. Pinal, I. Cervantes, and A. Emadi, "Stability of an electric differential for traction applications," *IEEE Trans. Veh. Technol.*, vol. 58, no. 7, pp. 3224–3233, Sep. 2009.

[16] B. Chen, C. Yu, W. Lee, and W. Hsu, "Design of an electric differential system for three-wheeled electric welfare vehicles with driver-in-the-loop verification," *IEEE Trans. Veh. Technol.*, vol. 56, no. 4, pp. 1498–1504, Jul. 2007.

[17] B. Tabbache, A. Kheloui, and M. Benbouzid, "An adaptive electric differential for electric vehicles motion stabilization," *IEEE Trans. Veh. Technol.*, vol. 60, no. 1, pp. 104–110, Jan. 2011.

[18] R. Wang, Y. Chen, D. Feng, X. Huang, and J. Wang, "Development and performance characterization of an electric ground vehicle with independently actuated in-wheel motors," *J. Power Sources*, vol. 196, no. 8, pp. 3962–3971, Apr. 2011.

[19] J. Y. Wong, *Theory of Ground Vehicles*. Hoboken, NJ: Wiley, 2008.

[20] R. Rajamani, *Vehicle Dynamics and Control*. New York: Springer-Verlag, 2006.

[21] K. H. Ang, G. Chong, and Y. Li, "PID control system analysis, design and technology," *IEEE Trans. Control Syst. Technol.*, vol. 13, no. 4, pp. 559–576, Jul. 2005.

[22] S. J. Ovaska and S. Väliviita, "Angular acceleration measurement: A review," *IEEE Trans. Instrum. Meas.*, vol. 47, no. 5, pp. 1211–1217, Oct. 1998.

Yan Chen received the B.E. and M.E. degrees in control science and engineering from the Harbin Institute of Technology, Harbin, China, in 2004 and 2006, respectively, and the M.S. degree in mechanical engineering and material science from Rice University, Houston, TX, in 2009. He is currently working toward the Ph.D. degree with the Vehicle Systems and Control Laboratory, Department of Mechanical and Aerospace Engineering, The Ohio State University, Columbus.

His research interests include modeling and control of nonlinear systems, energy-efficient control allocation, optimal control, and vehicle dynamics and control.

Junmin Wang (M'06) received the B.E. degree in automotive engineering and the M.S. degree in power machinery and engineering from Tsinghua University, Beijing, China, in 1997 and 2000, respectively, the second and third M.S. degrees in electrical engineering and mechanical engineering from the University of Minnesota, Twin Cities, in 2003, and the Ph.D. degree in mechanical engineering from the University of Texas, Austin, in 2007.

He has five years of full-time industrial research experience (May 2003–August 2008) at Southwest Research Institute, San Antonio, TX. Since September 2008, he has been an Assistant Professor with the Department of Mechanical and Aerospace Engineering, The Ohio State University, Columbus. He is an author/coauthor of over 100 peer-reviewed papers in journals and conference proceedings and is the holder of ten U.S. patents. His research interests include control, modeling, estimation, and diagnosis of dynamical systems, specifically for engine, powertrain, aftertreatment, hybrid, flexible fuel, alternative/renewable energy, (electric) ground vehicle, transportation, sustainable mobility, and mechatronic systems.

Dr. Wang is the Chair of the Society of Automotive Engineers (SAE) International Control and Calibration Committee and the Secretary of the American Society of Mechanical Engineers (ASME) Automotive and Transportation Systems Technical Committee for 2010–2012. He serves as an Associate Editor for the IEEE TRANSACTIONS ON VEHICULAR TECHNOLOGY, the Conference Editorial Board of the ASME Dynamic Systems and Control Division, the American Control Conference, and the ASME Dynamic Systems and Control Conference. He received the National Science Foundation CAREER Award in 2012, the SAE International Vincent Bendix Automotive Electronics Engineering Award in 2011, the Office of Naval Research Young Investigator Program Award in 2009, and the Oak Ridge Associated Universities Ralph E. Powe Junior Faculty Enhancement Award in 2009.